AD

TECHNICAL REPORT ARCCB-TR-03004

THERMAL DAMAGE, CRACKING, AND RAPID EROSION OF CANNON BORE COATINGS

JOHN H. UNDERWOOD
ANTHONY P. PARKER
GREGORY N. VIGILANTE
PAUL J. COTE

MARCH 2003

US ARMY ARMAMENT RESEARCH,
DEVELOPMENT AND ENGINEERING CENTER
Close Combat Armaments Center
Benét Laboratories
Watervliet, NY 12189-4000

DISCLAIMER

The findings in this report are not to be construed as an official Department of the Army position unless so designated by other authorized documents.

The use of trade name(s) and/or manufacturer(s) does not constitute an official endorsement or approval.

DESTRUCTION NOTICE

For classified documents, follow the procedures in DoD 5200.22-M, Industrial Security Manual, Section II-19, or DoD 5200.1-R, Information Security Program Regulation, Chapter IX.

For unclassified, limited documents, destroy by any method that will prevent disclosure of contents or reconstruction of the document.

For unclassified, unlimited documents, destroy when the report is no longer needed. Do not return it to the originator.

REPORT DOCUMENTATION PAGE

Form Approved
OMB No. 0704-0188

1. AGENCY USE ONLY *(Leave Blank)*	2. REPORT DATE	3. REPORT TYPE AND DATES COVERED
	March 2003	Final

4. TITLE AND SUBTITLE
THERMAL DAMAGE, CRACKING, AND RAPID EROSION OF CANNON BORE COATINGS

5. FUNDING NUMBERS
AMCMS No. 6226.24.H180.0
PRON No. TU1G1F261ABJ

6. AUTHORS
John H. Underwood, Anthony P. Parker (Royal Military College of Science, Cranfield University Swindon, UK), Gregory N. Vigilante, and Paul J. Cote

7. PERFORMING ORGANIZATION NAME(S) AND ADDRESS(ES)
U.S. Army ARDEC
Benet Laboratories, AMSTA-AR-CCB-O
Watervliet, NY 12189-4000

8. PERFORMING ORGANIZATION REPORT NUMBER
ARCCB-TR-03004

9. SPONSORING / MONITORING AGENCY NAME(S) AND ADDRESS(ES)
U.S. Army ARDEC
Close Combat Armaments Center
Dover, NJ 07806-5000

10. SPONSORING / MONITORING AGENCY REPORT NUMBER

11. SUPPLEMENTARY NOTES
Presented at Gun Tubes Conference 2002, Keble College, Oxford, UK, 15-18 September 2002.
Published in *Journal of Pressure Vessel Technology*.

12a. DISTRIBUTION / AVAILABILITY STATEMENT
Approved for public release; distribution unlimited.

12b. DISTRIBUTION CODE

13. ABSTRACT *(Maximum 200 words)*

Thermal damage observed at the bore of fired cannons has increased noticeably in the past decade, due to the use of higher combustion gas temperatures for improved cannon performance. Current authors and coworkers recently have described cannon firing damage and proposed new thermomechanical models to gain understanding of its causes, with emphasis on the severe damage that occurs in the steel *beneath* the chromium plating used to protect the cannon bore. Recent refinements in the models will be used here to characterize some additional damage observations in the area beneath the protective coating of fired cannons. Model results validated by microstructural observations give predictions of near-bore temperature and stress distributions and good agreement with observed depths of hydrogen cracking in the high-strength steel substrate.

Interest in damage and failure *within* a coating is also of concern for cannons, since coating failure leads to extremely rapid erosion of coating and substrate. The slip-zone model of Evans and Hutchinson is adapted here to predict failure strength of cannon coatings based on observed crack spacing and microhardness of thermally damaged areas. Results are described for electroplated chromium coatings from fired cannons and for sputtered chromium and tantalum coatings with laser-heating damage to simulate firing. Coating mechanics analysis of fired and laser-heated samples provides an in-situ measurement of coating failure strength, showing that sputtered chromium has more than twice the failure strength of electroplated chromium. An analysis of cyclic shear failure of a coating interface at an open crack shows a six-fold decrease in low-cycle fatigue life compared to the life of a closed crack. Recommendations are given for preventing rapid coating failure and catastrophic erosion of fired cannons, with emphasis on methods to prevent deep, open cracks in coating and substrate.

14. SUBJECT TERMS
Thermal Damage, Thermomechanical Model, Cannon Erosion, Cannon Coatings, Coating Failure

15. NUMBER OF PAGES
16

16. PRICE CODE

17. SECURITY CLASSIFICATION OF REPORT	18. SECURITY CLASSIFICATION OF THIS PAGE	19. SECURITY CLASSIFICATION OF ABSTRACT	20. LIMITATION OF ABSTRACT
UNCLASSIFIED	UNCLASSIFIED	UNCLASSIFIED	UL

TABLE OF CONTENTS

TABLES

LIST OF ILLUSTRATIONS

ACKNOWLEDGEMENTS

The authors are pleased to acknowledge the help of C. Rickard and C. Mulligan of Benet Laboratories, and G. A. Pflegl of Scientific Services Program, Battelle Columbus Laboratories, in the metallographic characterization described here.

INTRODUCTION

In the past decade the degree of thermal damage and associated erosion observed at the bore of fired cannons has increased noticeably, due to the use of higher combustion gas temperatures for improved cannon performance. Current authors and coworkers (refs 1,2) have described cannon firing damage and proposed new thermomechanical models to gain understanding of its causes, with emphasis on the severe damage that occurs in the high-strength steel *beneath* the chromium plating that protects the cannon bore. Recent refinements in the models will be used here to characterize some additional damage observations in the area beneath the protective coating of fired cannons. Model results are validated by microstructural observations and give predictions of near-bore temperatures and the transient and residual stresses that are produced by cannon firing. The depth of the critical near-bore tensile residual stress distribution is compared with the observed depth of hydrogen cracking in fired cannons, to help understand the factors that control cracking beneath the coating.

Interest in thermomechanical damage and failure *within* a coating is also of concern for many applications, including cannons where coating damage can lead to rapid erosion of coating and substrate. Evans and Hutchinson (ref 3) have presented a comprehensive review of the thermomechanical integrity of thin coatings, with particular application to the electronics industry. Their slip-zone model of a cracked coating is adapted here to predict failure strength of cannon coatings based on observed crack spacing and microhardness in the thermally damaged area. Results are described for electroplated chromium coatings from fired cannons and for sputtered chromium and tantalum coatings with simulated firing damage. The thermal loads of firing are simulated with laser-pulse heating of coated samples using the few millisecond pulse duration typical of cannon firing (ref 4). Coating mechanics analysis of fired and laser-heated samples provides a unique in-situ measurement of coating failure strength under the actual thermal damage conditions—damage that both modifies the properties of the coating and applies thermal loading to it. Such tests and analyses provide a ranking of in-situ coating failure strength that can have important use in design of erosion-resistant coatings for cannons.

CANNON FIRING DAMAGE

Near-bore thermomechanical damage is characterized here in a fired 120-mm tank cannon of the same type as that described in earlier work (refs 1,2). The earlier cannon firing (tube #26) used experimental rounds that are believed to represent an upper bound of thermal damage for this type of cannon, whereas the recent firing (tube #12) is believed to have imparted more typical damage. Thus, taken together, the information from these firings provides a useful description of the firing damage that can be expected in 120-mm tank cannons. Figure 1 shows a longitudinal metallographic section of the near-bore damage from the recent firing of 120-mm tube #12 at the axial location 0.7-m forward from the breech end of the tube. This location of the bore surface is the closest to the cannon chamber where the combustion gas is hottest, so significant thermal damage is expected.

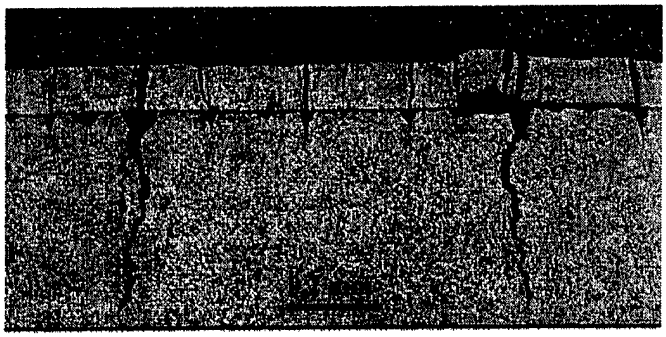

Figure 1. Cannon firing damage in 120-mm tube #12 at 0.7-m location, longitudinal section.

The basic features of the damage shown in Figure 1 are the same as those seen in the earlier work. The electrodeposited chromium coating (light area near the top of the photomicrograph) and the underlying ASTM A723 steel substrate are severely cracked, with many cracks opened significantly and some "islands" of chromium near complete failure. Note the separation of the chromium islands that are adjacent to the dominant substrate crack on the right of Figure 1. Prior analysis of stresses applied to chromium islands (ref 5) indicated that thermal-expansion-driven shear failure of islands adjacent to deep, open cracks is a likely cause of island failure and separation. The island failure shown in Figure 1 is directly adjacent to a deep, open crack and is thus consistent with this prior analysis. Another common feature with the current and earlier work is the nearly constant 0.5-mm depth array of dominant cracks in the steel substrate. The two such cracks shown in Figure 1 are typical of those observed at the 0.7-m location of tube #12. Finally, evidence of steel transformation and chromium recrystallization and grain growth were seen in tube #12 as in the earlier work, but neither is clear in Figure 1 because the metallographic preparation for the figure was intended to highlight cracking rather than transformation. Some of these key thermal damage features of the current tube #12 are compared with the prior tube #26 in Table 1. The chromium thickness and observed transformation depths and crack depths will be used as inputs and comparisons in the upcoming description of model results.

Table 1. Near-Bore Thermal Damage and Model Results

Chromium Thickness	Transformation Depth		Model Calculations			Crack Depth		Heat Input
	Steel	Chromium	Δt	T_{GAS}	T_{ID}	Obser.	Model	
(mm)	(mm)	(mm)	(ms)	(°K)	(°K)	(mm)	(mm)	(J/mm^2)
#12 0.10	0.14	0.06	4.1	2490	1470			
			9.5	1740		0.53	0.46	1.28
#26 0.12	0.19	0.08	4.1	3310	1890			
			9.5	1990		0.46	0.50	1.51

The cause and driving force of thermal damage in cannons is the temperature and duration of the combustion gases produced during firing. In prior analysis, a representative constant time duration was chosen and gas temperature was varied until the near-bore temperatures matched those of the observed transformations. In the work here, different values of time duration will be considered, based on the information in Figure 2. Results are shown of an interior ballistics model (ref 6) of gas temperature for 120-mm cannon firing at the 0.7-m location. After rising quickly to a maximum of 3170°K, the gas temperature reduces so that the time durations at two-thirds and one-half of the maximum temperature, $\Delta t_{2/3}$ and $\Delta t_{1/2}$, are 4.1- and 9.5-ms, respectively. These time durations will be used in the upcoming model of near-bore temperatures and stresses for the 120-mm tube. The duration $\Delta t_{2/3}$ is expected to be more appropriate for modeling very near-bore behavior, such as the bore temperature, T_{ID}, whereas $\Delta t_{1/2}$ is expected to be more appropriate for modeling the behavior further removed from the bore, such as the applied and residual stresses in the steel substrate beneath the coating.

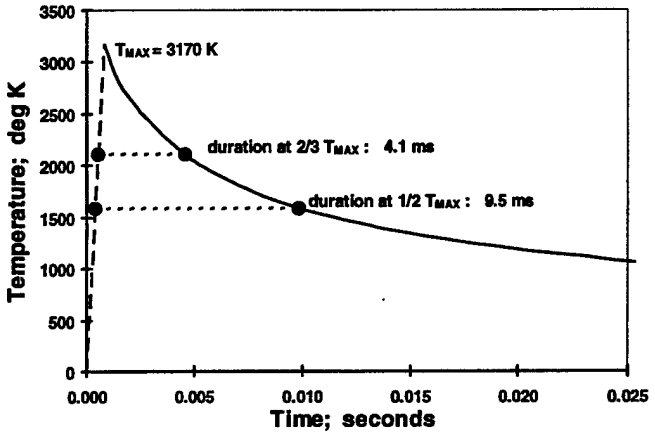

Figure 2. Interior ballistics model calculation of gas temperature for 120-mm cannon at 0.7-m location

SUBSTRATE DAMAGE MODEL AND RESULTS

The basis of the damage model (refs 1,2) is the near-bore temperature distribution obtained by finite-difference temperature calculations. One-dimensional heat flow spread-sheet calculations were performed here, using increments of about 0.02-mm in depth below the heated bore surface. About fifty increments were required for the temperature to drop from typically 1500°K at the surface to within 1°K of ambient at about 1-mm below the surface. Temperature-dependent thermal properties of bulk chromium and tantalum and the ASTM A723 steel substrate (ref 2) were used for the analysis, in the form $fn(T) = C_0 + C_1T$; see Table 2. The mechanical properties of A723 steel used were:

- Elastic modulus, $E = 248 - 0.097T$, in GPa
- Poisson's ratio, $\nu = 0.3$
- Thermal expansion, $\alpha = 13.5E\text{-}6$, in $°K^{-1}$
- Yield strength, $S_Y = 1450 - 1.16T$, in MPa

Temperature, T, is in °K. The inputs to the finite-difference calculations, in addition to the chromium and steel properties, were:

- The thickness of the coating
- The initial ambient temperature, $T_i = 300°K$
- The duration of the convective heating pulse at the tube surface, 0.0041 and 0.0095-s, as has been discussed
- The convection coefficient of the heating pulse, $h = 193{,}000$ W/m^2°K
- The mean gas temperature of the pulse, T_{GAS}, with values as discussed in the upcoming results

Table 2. Properties of Coatings and Substrate

	Thermal Diffusivity (δ, m^2/s)		Thermal Conductivity (k, W/m°K)	
Valid For:	C_0 (300-2000°K)	C_1	C_0 (300-2000°K)	C_1
Chromium	29.6E-6	-12.6E-9	97.2	-0.0266
Tantalum	25.1E-6	-1.20E-9	56.3	-0.0039
Steel	11.7E-6	-5.30E-9	43.6	-0.0097

Expressions for the near-bore, transient, in-plane, biaxial compressive thermal stress, S_T, and the tensile residual stress, S_R, produced in the steel substrate when the transient stress exceeds the steel yield strength, are as follows:

$$S_T = -Ea[T\{x,\Delta t\} - T_i]/[1 - \nu] \quad (1)$$

$$S_R = -S_T - S_Y \qquad for\ S_T > S_Y \quad (2)$$

where the transient temperature, $T\{x,\Delta t\}$, from the finite-difference calculations is for a given depth, x, below the bore surface and duration, Δt, of a heating pulse; the term $[1 - \nu]$ accounts for the biaxial nature of the temperature and stress distributions. The value of S_R is determined using the linear unloading concept, in which a residual stress is created by a virtual unloading from a calculated elastic applied stress (thermal in this case) that is envisioned to be above the yield level of the material. The residual stress is of opposite sense to the applied stress and of a value equal to the difference between the applied stress and the yield strength, as shown by equation (2).

The model results for fired 120-mm cannon #12 at the 0.7-m location are shown in Figure 3. The temperature distribution for $\Delta t_{1/2} = 4.1$-ms drops from 1470°K at the bore surface, passes

near the approximate 1320°K chromium recrystallization temperature (ref 1) at the 0.06-mm observed depth, changes slope as expected at the chromium-steel interface at 1190°K, and passes through the chosen validation point, the 1020°K steel transformation temperature (ref 1) at the 0.14-mm observed depth. Referring again to Table 1, the gas temperature that matches model results with the observed steel transformation is 2490°K for the 4.1-ms duration results in Figure 1 and 1740°K for 9.5-ms duration. Note that these gas temperatures are quite consistent with the results in Figure 2 for the respective time durations. This consistency check, along with the validation by steel transformation results, gives confidence in the use of model temperatures for calculating stresses, discussed next.

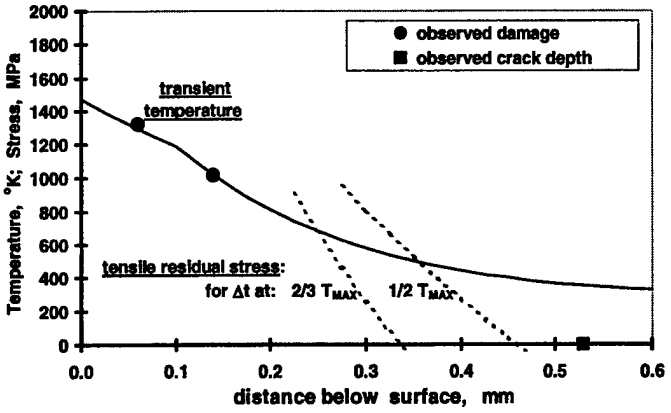

Figure 3. Thermomechanical model results for fired cannon #12 at 0.7-m location.

Near-bore temperatures were used to calculate the significant compressive transient stresses for tube #12, and from these stresses, the tensile residual stresses, as outlined by equations (1) and (2). Tensile residual stress results for each of the time durations, 4.1- and 9.5-ms, and their respective gas temperatures, 2490 and 1740°K, are shown in Figure 3. Even though the longer duration had a significantly lower gas temperature, the result was a deeper penetration of tensile residual stress, which also was in better agreement with the observed crack depth. Similar calculations were performed for tube #26, with somewhat higher temperatures and deeper penetration of tensile residual stress. Note the corresponding higher heat input for #26 compared with #12, 1.51 and 1.28 J/mm^2, respectively. These values will have use in comparing the intensity of thermal loading for cannon firing considered thus far with the laser-heating simulation of cannon firing considered in upcoming sections.

A brief summary of proposed key mechanisms of cannon coating and substrate firing damage suggested by the work here and other related work (refs 1,2,5,6) follows. Hot cannon combustion gases first cause extreme thermal expansion and compressive yielding of the chromium coating and the near-bore region of the steel substrate. Upon cooling, tensile residual stresses in both chromium and steel cause brittle cracking of the chromium, thereby exposing the steel to the significant hydrogen component of the combustion gases, leading to hydrogen cracking of the steel. The deeper hydrogen cracks in the steel lead to widening of cracks in both

steel and chromium, which accelerates the shear failure of chromium islands, the critical final event in the failure of the cannon coating.

The remaining work here addresses the use and modeling of laser heating as a simulation of firing damage of cannon coatings, with emphasis on the aforementioned key mechanisms of coating damage.

LASER-HEATING DAMAGE

A procedure for laser-pulse heating of coated samples has been developed to simulate the thermal damage that occurs at a cannon bore (ref 4). Figures 4 and 5 show metallographic sections of laser-heated A723 steel samples coated with sputtered chromium and tantalum, respectively. Each of the samples was subjected to twenty 5-ms pulses of laser heating of about 1 J/mm^2 heat input. Referring again to Figure 2, 5-ms is the typical duration of a cannon firing pulse.

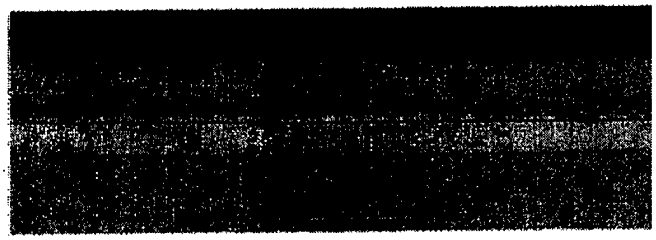

Figure 4. Laser-pulse heating of sputtered chromium on A723 steel.

Figure 5. Laser-pulse heating of sputtered tantalum on A723 steel.

The general nature of the laser thermal damage is similar in Figures 4 and 5. Cracking and metallurgical transformation damage occurs in the coating, and transformation occurs in the steel substrate in each of the two samples. Significant cracking of the steel, as in Figure 1, is not seen. This lack of steel cracking cannot be explained by less severe thermal damage, since, as will be discussed, the laser thermal damage is comparable to the firing thermal damage. The lack of steel cracking is believed due to the lack of other than trace amounts of hydrogen during laser heating, compared with up to 10 volume % hydrogen at up to 70 MPa partial pressure in cannon firing gases (ref 2).

The metallurgical transformations that can be seen in Figures 4 and 5 are interesting as well as useful for performing and validating the thermomechanical modeling. Evidence of recrystallization and grain growth to a depth of about two-thirds of the chromium thickness can

be seen in Figure 4. This provides a known depth for the 1320°K characteristic temperature for this transformation, for use in modeling. A thin band of an apparent transformation can be seen at the interface of the tantalum-coated, laser-heated sample shown in Figure 5. This is believed to be evidence of the 1715°K eutectic transformation in tantalum-iron alloys. Upcoming results will support this contention. A summary of the observed thermal damage in the laser-heated coated samples is given in Table 3, along with some thermomechanical model results for these samples, considered next.

Table 3. Thermal Damage and Model Results for Laser-Heated Coated Samples

Coating Thickness (mm)	Transformation Depth		Maximum ID Temperature	Crack Depth		Heat Input
	Steel (mm)	Coating (mm)	(°K)	Obser. (mm)	Model (mm)	(J/mm^2)
Chromium: 0.09	0.14	0.06	1400	None	0.35	1.07
Tantalum: 0.07	0.20	0.07	1900	None	0.40	1.41

Model temperature and stress distributions for the laser-heated samples are shown in Figures 6 and 7. Gas temperatures of 2240 and 3020°K, respectively, were input to the model to provide heat input equivalent to laser heating. Equivalency was verified by matching the observed steel transformation depths shown in Table 3. Other inputs were:

- The coating and steel properties and the thickness of the coatings from Tables 2 and 3
- The initial ambient temperature, $T_i = 300°K$
- The 5-ms duration of the laser-heating pulse
- The equivalent convection coefficient of the heating pulse, $h = 193{,}000\ W/m^{2o}K$

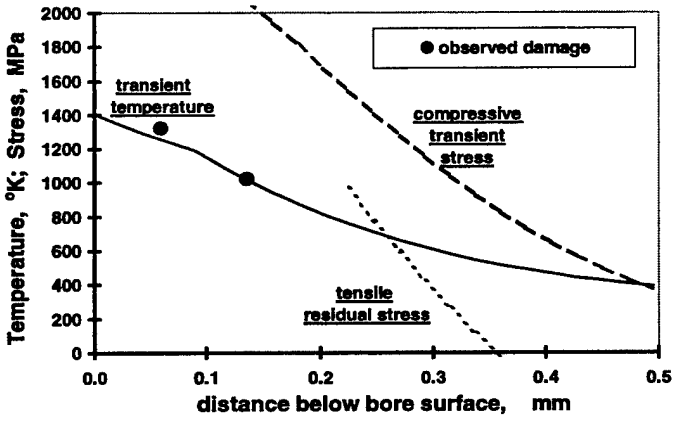

Figure 6. Thermomechanical model results for laser-heated chromium on A723 steel.

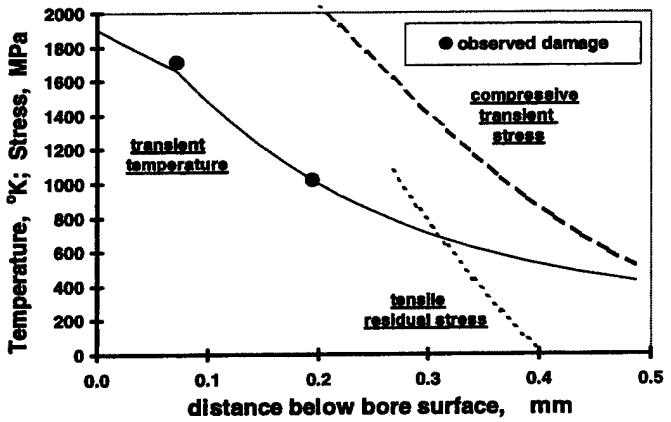

Figure 7. Thermomechanical model results for laser-heated tantalum on A723 steel.

Note that the temperature distribution in both Figures 6 and 7 passes close to the observed depth and known temperature of the transformation damage in the respective coating, thus verifying the model temperature results. The finite-difference calculations also give the heat input that corresponds to the model temperatures. See Table 3. The temperatures are used to calculate the compressive transient and tensile residual stresses using equations (1) and (2). In the cannon firing results of Figure 3, the depth of tensile residual stress was seen to approximately match the observed depth of the hydrogen cracking. In the laser-heating results of Figures 6 and 7, tensile residual stresses are 0.35- to 0.40-mm deep, but there was no hydrogen present and thus no cracks observed, as has been discussed.

Finally, it is interesting to compare cannon firing results in Figure 1 with laser-heating results in Table 3. The results are quite similar, including the observed transformation depths, the inner diameter (ID) temperatures, and the heat inputs. It is clear that, apart from the lack of cracks in the steel beneath the coating, these laser-heating tests gave a close simulation of the thermomechanical damage sustained by the cannon bore during firing.

COATING DAMAGE MODEL AND RESULTS

The critical first step in the thermal firing damage at a cannon bore is the initial cracking of the coating. If the coating were to remain intact, much of the damage under discussion here would be prevented or at least significantly delayed. So the first cracking of a cannon coating is worthy of attention. Evans and Hutchinson (ref 3) have presented a comprehensive review of the thermomechanical integrity of thin coatings with particular application to typically 1-μm thick electronic coatings. Notwithstanding the 10^2 difference in thickness between cannon and electronic coatings, their slip-zone model of a cracked coating can be adapted here to predict failure strength of cannon coatings. A cannon coating is still very thin relative to a cannon wall thickness, typically 100-mm or more.

The concepts of the Evans/Hutchinson slip-zone model, as adapted to the determination of the tensile failure strength of the coating, are shown in Figure 8. A preexisting through-thickness crack in the cannon coating is envisioned and easily justified, considering the large area of a cannon ID and its severe service environment. The tensile residual stress, σ_R, in the coating of thickness, t, is relieved at the crack site and the load formerly carried by the coating is now carried by a shear zone of length, L, on either side of the crack.

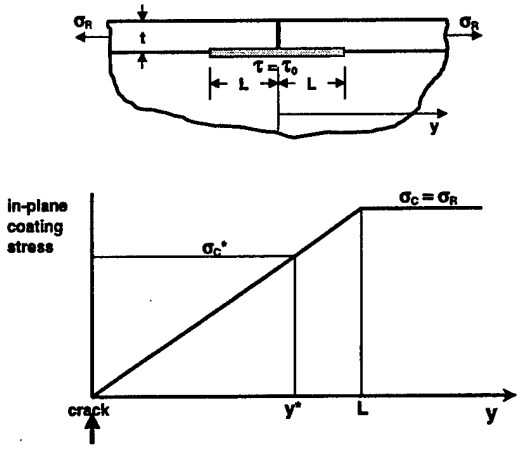

Figure 8. Evans/Hutchinson interface slip-zone adapted for tensile failure of cannon coatings.

An expression that equates the load in terms of tensile residual stress to that in terms of the minimum shear yield strength near the interface, τ_0, and dimensions t and L is

$$\sigma_R t = \tau_0 L \tag{3}$$

Using this expression and the concept (sketch in Figure 8) that the in-plane tensile stress in the coating increases linearly with distance, y, away from the crack location, leads to

$$y^*/t = \sigma_C^*/\tau_0 \tag{4}$$

where y^* is the critical crack spacing away from a preexisting crack at which the coating stress reaches the tensile failure strength of the coating material, σ_C^*. It can be seen from equation (4) that the observed crack spacing in the coating and the measured minimum shear strength near the interface provide a measure of the tensile failure strength of the coating. This has clear importance to design and development of coatings, particularly so for cannon coatings in which the in-situ properties can be so affected by thermal damage, as shown here. A metallographic cross-section, such as Figures 1, 4, and 5, can be used to determine y^* directly and τ_0 indirectly, using microhardness tests. Note the Vickers hardness indentations in Figure 4. The following discussion of coating damage results uses Knoop microhardness measurements.

Table 4 lists the information used to calculate coating failure strength, including the coating thickness, the hardness near the interface, and the crack spacing. The minimum hardness near the interface was always that of the coating, compared to the untempered martensite beneath the interface. The following correlation between Knoop hardness, HK, and shear yield strength,

τ_0, was used: $\tau_0 = 1.57$ HK. Although this expression is based on hardness results for steels, it provides a good estimate for chromium and tantalum shear strengths. The crack spacing normalized by t in Table 4 is the mean of a series of measurements from photos such as Figures 1, 4, and 5. The coating strengths that result from the measurements and analysis show that sputtered chromium has more than twice the failure strength of electroplated chromium, whereas sputtered tantalum has a strength intermediate to that of the two types of chromium.

Table 4. Coating Characterization and Predicted Failure Strength

Coating	Coating Thickness (t, mm)	Crack Spacing (y^*/t)	Interface Hardness (HK)	Shear Strength (τ_0, MPa)	Failure Strength (σ_C^*, MPa)
Chromium Plate #26	0.12	1.2	370	580	700
Chromium Plate #12	0.10	1.0	410	640	640
Chromium Sputtered	0.09	2.5	440	700	1730
Tantalum Sputtered	0.07	2.9	220	350	1000

A final topic in damage mechanics of coatings relates to cyclic shear failure near the coating interface. The earlier description of the separation of the chromium islands shown in Figure 1 stressed the importance of open cracks in the *rising-load* shear failure of coating segments (ref 5). Related mechanisms of *cyclic* shear failure of coatings and the important role of open cracks in cyclic failure are described in Figure 9. The top sketch shows the interface shear zone and associated shear stresses near an open crack in a coating containing tensile residual stress. One can arbitrarily assign a positive sign to these shear stresses. Then consider, in the bottom sketch, the thermal expansion and high compressive stress that occurs during the next cannon firing. A deep, sufficiently open crack will remain open during the thermally driven compression, and the interface shear stresses will reverse in sign. Whereas, had the crack closed, the reversal of shear stress would have been prevented or lessened. Recall from Figure 1 the large crack opening at the site of island failure of the coating.

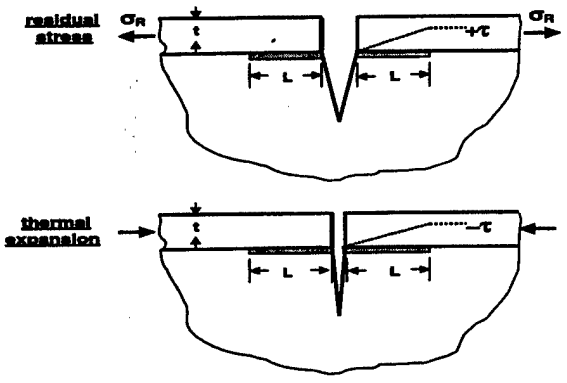

Figure 9. Cyclic shear failure of coating interface at an open crack site.

This concept, that the shear stress for an open crack can reverse and thereby double the range of shear stress, can be used in calculations of the shear fatigue life of a coating island. Reference 8 describes the use of Coffin-Manson low-cycle fatigue life expressions for an 1100 MPa tensile strength steel, repeated here as

$$\Delta\varepsilon_T/2 = 0.63(2N)^{-0.072} + 78.25(2N)^{-0.675} \qquad (5)$$

Using $\Delta\varepsilon_T = 1\%$ as a total strain range for the case of a closed crack and $\Delta\varepsilon_T = 2\%$ for the case of reversed shear strain at an open crack gives calculated fatigue lives of

- $N = 4300$ cycles; closed crack
- $N = 640$ cycles; open crack

This is a nearly seven-fold reduction in life for an open crack. Low-cycle fatigue life is controlled by shear stresses, so this concept of open-crack doubling of shear stress range provides improved understanding of the failure mechanisms of cannon bore coatings.

CONCLUSIONS

The experimental observations and the results of analysis described here lead directly to the following conclusions:

1. Deep, open cracks are a preferred site of island failure of electroplated chromium at the bore of a fired cannon, in agreement with prior observations.

2. Variation of heating-pulse duration in the thermomechanical modeling of cannon firing shows that the first 4-ms of the pulse with higher mean temperature has primary control of initial coating damage, whereas a longer 10-ms pulse with lower mean temperature gives a better description of total heat input and depth of tensile residual stress and associated hydrogen cracking.

3. Laser heating of coated gun steel samples gives an excellent simulation of cannon bore thermal damage, as shown by metallographic evidence of steel, chromium, and tantalum transformations; similar cracking observations in coatings; and similar temperatures and heat inputs from analysis.

4. Laser-heated samples showed no significant cracking of the steel beneath the coating, in contrast to the deep hydrogen cracks in fired cannons. This is consistent with only trace amounts of hydrogen present during laser heating, compared with the significant presence of hydrogen in cannon firing gases.

5. The Evans/Hutchinson slip-zone model was adapted to determine the in-situ tensile failure strength of coatings, based on measured crack spacing and microhardness in thermally damaged areas from fired cannons and laser-heating tests. Results show that sputtered chromium coatings have more that twice the failure strength of electroplated chromium coatings.

6. Mechanics analysis of the low-cycle shear fatigue life of cannon coatings shows a seven-fold decrease in life for a coating segment adjacent to a deep, open crack, compared to the life adjacent to a shallower crack that can close.

Some general conclusions can be drawn from the results here and previous related results, with emphasis on potential solutions to thermal damage problems in cannons. First, the deep, open hydrogen cracks that grow *beneath* the cannon coating could be discouraged by:

- Increasing the coating failure strength, to lessen coating cracks and slow passage of hydrogen to the substrate
- Adding an interlayer such as nickel between coating and substrate, to block passage of hydrogen
- Decreasing the strength and carbon content of a near-bore layer of the steel substrate, to decrease the susceptibility of the steel to hydrogen cracking

Second, the through-thickness cracks *within* the coating could be discouraged by:

- Increasing the coating failure strength as-applied or after application by post-treatment
- Decreasing the shear stress transfer between coating and substrate, by using a softer coating, adding a soft interlayer, or softening the near-interface layer of the steel substrate

REFERENCES

1. Underwood, J.H., Parker, A.P., Cote, P.J., and Sopok, S., "Compressive Thermal Yielding Leading to Hydrogen Cracking in a Fired Cannon," *Journal of Pressure Vessel Technology,* Vol. 121, 1999, pp.116-120.

2. Underwood, J.H., Vigilante, G.N., and Troiano, E., "Failure Beneath Cannon Thermal Barrier Coatings by Hydrogen Cracking; Mechanisms and Modeling," *Fatigue and Fracture Mechanics: 33rd Volume, ASTM STP 1417,* (W.G. Reuter and R.S. Piascik, eds.), American Society for Testing and Materials, West Conshohocken, PA, 2002.

3. Evans, A.G., and Hutchinson, J.W., "The Thermomechanical Integrity of Thin Films and Multilayers," *Acta Metallurgica et Materialia*, Vol. 43, 1995, pp. 2507-2530.

4. Cote, P.J., Kendall, G., and Todaro, M.E., "Laser Pulse Heating of Gun Bore Coatings," *Surface and Coatings Technology*, September 2001, pp. 65-69.

5. Underwood, J.H., and Parker, A.P., "Thermal Damage and Shear Failure of Chromium Plated Coating on an A723 Steel Cannon Tube," *Advances in Life Prediction Methodology, PVP-391,* (R. Mohan, ed.), ASME, New York, 1999.

6. Sopok, S., O'Hara, P., Vottis, P., Pflegl, G., Rickard, C., and Loomis, R., "Erosion Modeling of the 120-MM M256/M829A2 Gun System," *Proceedings of 1997 ADPA* Gun *and Ammunition Symposium*, San Diego, CA, 7-10 April 1997.

7. Massalski, T.B., ed., *Binary Alloy Phase Diagrams, Second Edition*, ASM International, 1990, p. 1777.

8. Truchon, M. "Application of Low-Cycle Fatigue Test Results to Crack Initiation from Notches," *Low-Cycle Fatigue and Life Prediction, ASTM STP 770,* ASTM, 1982, pp. 254-268.

TECHNICAL REPORT INTERNAL DISTRIBUTION LIST

	NO. OF COPIES
TECHNICAL LIBRARY ATTN: AMSTA-AR-CCB-O	1
TECHNICAL PUBLICATIONS & EDITING SECTION ATTN: AMSTA-AR-CCB-O	3
PRODUCTION PLANNING & CONTROL DIVISION ATTN: AMSTA-WV-ODP-Q, BLDG. 35	1

NOTE: PLEASE NOTIFY DIRECTOR, BENÉT LABORATORIES, ATTN: AMSTA-AR-CCB-O OF ADDRESS CHANGES.

TECHNICAL REPORT EXTERNAL DISTRIBUTION LIST

	NO. OF COPIES
DEFENSE TECHNICAL INFO CENTER ATTN: DTIC-OCA (ACQUISITIONS) 8725 JOHN J. KINGMAN ROAD STE 0944 FT. BELVOIR, VA 22060-6218	2
COMMANDER U.S. ARMY ARDEC ATTN: AMSTA-AR-WEE, BLDG. 3022 AMSTA-AR-AET-O, BLDG. 183 AMSTA-AR-FSA, BLDG. 61 AMSTA-AR-FSX AMSTA-AR-FSA-M, BLDG. 61 SO AMSTA-AR-WEL-TL, BLDG. 59 PICATINNY ARSENAL, NJ 07806-5000	1 1 1 1 1 2
DIRECTOR U.S. ARMY RESEARCH LABORATORY ATTN: AMSRL-DD-T, BLDG. 305 ABERDEEN PROVING GROUND, MD 21005-5066	1
DIRECTOR U.S. ARMY RESEARCH LABORATORY ATTN: AMSRL-WM-MB (DR. B. BURNS) ABERDEEN PROVING GROUND, MD 21005-5066	1
CHIEF COMPOSITES & LIGHTWEIGHT STRUCTURES WEAPONS & MATLS RESEARCH DIRECT U.S. ARMY RESEARCH LABORATORY ATTN: AMSRL-WM-MB (DR. BRUCE FINK) ABERDEEN PROVING GROUND, MD 21005-5066	1

	NO. OF COPIES
COMMANDER U.S. ARMY RESEARCH OFFICE ATTN: TECHNICAL LIBRARIAN P.O. BOX 12211 4300 S. MIAMI BOULEVARD RESEARCH TRIANGLE PARK, NC 27709-2211	1
COMMANDER ROCK ISLAND ARSENAL ATTN: SIORI-SEM-L ROCK ISLAND, IL 61299-5001	1
COMMANDER U.S. ARMY TANK-AUTMV R&D COMMAND ATTN: AMSTA-DDL (TECH LIBRARY) WARREN, MI 48397-5000	1
COMMANDER U.S. MILITARY ACADEMY ATTN: DEPT OF CIVIL & MECH ENGR WEST POINT, NY 10966-1792	1
U.S. ARMY AVIATION AND MISSILE COM REDSTONE SCIENTIFIC INFO CENTER ATTN: AMSAM-RD-OB-R (DOCUMENTS) REDSTONE ARSENAL, AL 35898-5000	2
NATIONAL GROUND INTELLIGENCE CTR ATTN: DRXST-SD 2055 BOULDERS ROAD CHARLOTTESVILLE, VA 22911-8318	1

NOTE: PLEASE NOTIFY COMMANDER, ARMAMENT RESEARCH, DEVELOPMENT, AND ENGINEERING CENTER, BENÉT LABORATORIES, CCAC, U.S. ARMY TANK-AUTOMOTIVE AND ARMAMENTS COMMAND, AMSTA-AR-CCB-O, WATERVLIET, NY 12189-4050 OF ADDRESS CHANGES.

DEPARTMENT OF THE ARMY
ARMAMENT RESEARCH, DEVELOPMENT AND ENGINEERING CENTER
BENÉT LABORATORIES, CCAC
US ARMY TANK-AUTOMOTIVE AND ARMAMENTS COMMAND
WATERVLIET, NY 12189-4000

OFFICIAL BUSINESS
AMSTA-AR-CCB-O
TECHNICAL LIBRARY